nature communications

Article

https://doi.org/10.1038/s41467-025-59697-z

Configurable kinetics of polarization switching via ion migration in ferroionic $CuInP_2S_6$

Received: 6 November 2024

Accepted: 1 May 2025

Published online: 14 May 2025

Check for updates

Lei Liang[1,2,9], Er Pan[1,9], Guiming Cao[3,4,9] ✉, Jiangang Chen[1], Ruixue Wang[1,5,6], Biao Dong[1,2], Qing Liu[1], Xiong Chen[7], Xiao Luo[1], Yongfa Kong[2], Wenwu Li[5,6] ✉ & Fucai Liu[1,8] ✉

Ferroelectric materials are promising for developing non-volatile memory, neuromorphic computing, and photovoltaic technologies. Taking advantage of variable switching kinetics provides an important strategy for designing multifunctional ferroelectric devices. However, the conventional ferroelectrics due to the unmovable atomic species generally own a single switching kinetics, thus versatile and configurable switching kinetics still remain challenging. In this work, we systematically investigate the switching kinetics of the van der Waals ferroionic $CuInP_2S_6$ through polarization-determined ferroelectric photovoltaic behaviors. Based on the time- and field-dependent polarization switching and numerical simulation, we discover three switching modes, including intralayer switching, interlayer switching and intralayer-interlayer coupling switching in $CuInP_2S_6$. Through designing the poling voltage amplitude and width, we achieve the configurable kinetic control of polarization switching in $CuInP_2S_6$, enabling tunable binary, gradual and accumulative switching with defined poling voltages in a single device. The work demonstrated here is instructive for the development of nanoscale multifunctional ferroelectric devices.

Beneficial from the switchable spontaneous polarization with external stimuli, ferroelectrics are holding great promise for numerous devices, i.e., non-volatile memory[1–3], logic device[4–7], actuators[8–10], and ferroelectric photovoltaic (FePV) applications[11–16]. The inherent nature of ultrafast switching, ultralow power consumption, and ultrahigh retention makes ferroelectrics highly potential for developing energy-efficient neuromorphic computing, overcoming the Von Neumann bottleneck. To meet the unprecedented device requirements of increased storage density, mimicking complex neuromorphic dynamics, as well as overcoming the intrinsic bi-stability, diverse switching kinetics have been designed based on various material phases and structures, enabling a plethora of ferroelectric devices[17–21]. Taking advantage of polarization switching kinetics has provided a promising solution for designing novel multifunctional ferroelectric devices.

Based on the theory of nucleation and domain growth, polarization switching kinetics is typically characterized by a waiting time (t_0)

[1]School of Optoelectronic Science and Engineering, University of Electronic Science and Technology of China, Chengdu 611731, China. [2]School of Physics, Nankai University, Tianjin 300071, China. [3]School of Information Science and Technology, Xi Chang University, Xi Chang 615013, China. [4]Key Laboratory of Liangshan Agriculture Digital transformation of Sichuan Provincial Education Department, Xi Chang University, Xi Chang 615013, China. [5]Shanghai Frontiers Science Research Base of Intelligent Optoelectronics and Perception, Institute of Optoelectronics, Fudan University, Shanghai 200433, China. [6]State Key Laboratory of Photovoltaic Science and Technology, Department of Materials Science, Fudan University, Shanghai 200433, China. [7]Faculty of Electronic and Information, Xi'an Jiaotong University, Xi'an 710049, China. [8]State Key Laboratory of Electronic Thin Films and Integrated Devices, University of Electronic Science and Technology of China, Chengdu 611731, China. [9]These authors contributed equally: Lei Liang, Er Pan, Guiming Cao.
✉e-mail: guimingcao@xcc.edu.cn; liwenwu@fudan.edu.cn; fucailiu@uestc.edu.cn

of nucleation and/or domain coalescence. When domain coalescence dominates the polarization reversal process, polarization switching follows domain-wall-motion mechanism (Fig. 1a, e and Supplementary Note 1), and is well described by the Kolmogorov–Avrami–Ishibashi (KAI) model[22]. While nucleation dominates the polarization reversal process (Fig. 1b, f), the nucleation-limited-switching (NLS) model is responsible for switching kinetics[23]. These statistic characteristics of domain nucleation and coalescence gives rise to various switching processes, and thus enable different device applications. For example, the switching time for domain coalescence in a single crystal is nearly constant, and thus a binary digital switching that the adopted pulse width is either insufficient to reverse the polarization or deterministic for switching completely, is easy to trigger, facilitating the non-volatile memory. While the statistics of nucleation in polycrystalline ferroelectrics is a Lorentz distribution function, providing an efficient way to achieve multiple polarization states that are necessary for synapse mimicking. In addition, designing a multi-peak distribution function, such as in ferroelectric superlattices, even makes controlled layer-by-layer switching of individual ferroelectric layers feasible (Fig. 1c, g), paving way for realizing multi-level non-volatile memory[24]. To date, although various switching kinetics have been designed for constructing different functional ferroelectric devices, the device with specific ferroelectric materials and architecture generally owns a single switching kinetics (Fig. 1a–c). Alternatively, achieving configurable kinetics control of polarization switching in a pre-defined material or device holds great potential for enriching ferroelectric device applications, but remains a significant challenge, as the switching process is usually initiated at crystal boundaries or defects, closely related to the crystal phase/structure.

Van der Waals (vdW) layered ferroionic $CuInP_2S_6$ (CIPS) owns the unique coupling effect of ferroelectricity and ionic conductivity[25–32]. Importantly, polarization switching and ionic migration cross the vdW gaps are both derived from Cu ions hopping progress[33–35]. Notably, the interlayer crossing of Cu ions even enables polarization aligns against the applied electric field (Fig. 1d, h). These extraordinary physical characteristics make CIPS a potential platform for exploring rich polarization switching processes and developing configurable multifunctional ferroelectric devices. However, the huge leakage current, resulting from ion current with Cu ions long-term migration and electron current with electrons drift or tunneling, hinders the switching kinetics exploring in CIPS thin films[2,36–39]. In this work, making use of polarization-determined FePV behaviors, and systematically investigating polarization switching

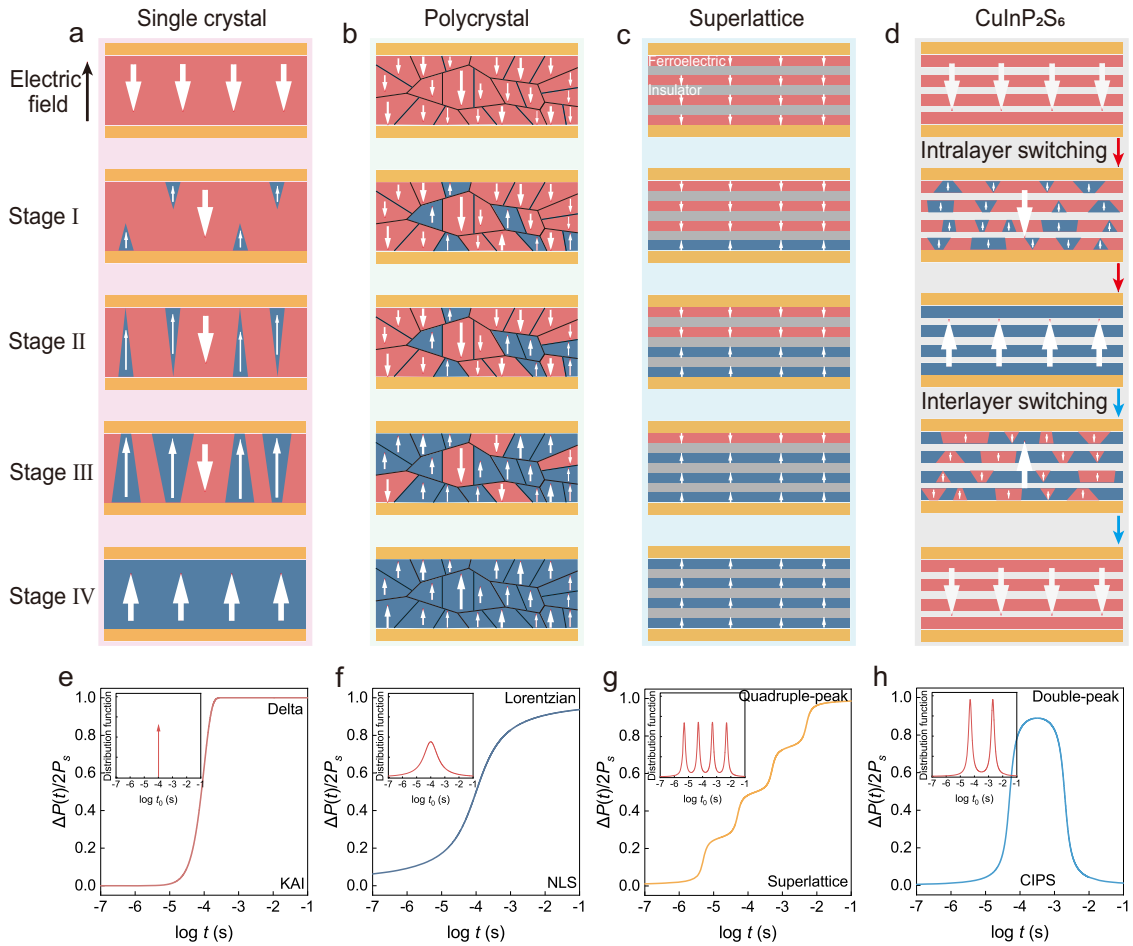

Fig. 1 | Progress of polarization switching in different ferroelectrics. a Diagram of polarization switching in a single crystal, where domain coalescence dominates the switching process and is described by the KAI model. **b** Diagram of polarization switching in polycrystalline ferroelectrics, where domain nucleation dominates the switching process and follows the NLS model. **c** Diagram of polarization switching in ferroelectric superlattice, where individual ferroelectric layers can be switched layer-by-layer. **d** Diagram of anomalous polarization switching in CIPS. While Cu ions undergo intralayer hopping and interlayer hopping progress during the migration, polarization alignment with and against the applied electric field occurs sequentially. **e** Time-dependent changing polarization of KAI model, with a constant of switching time t_0. **f** Time evolution of changing polarization based on the NLS model, where switching time is characterized by the Lorentzian function. **g** Time-dependent changing polarization in ferroelectric superlattices, where a quadruple-peak function determined by four individual ferroelectric layers is responsible for the distribution of switching time. **h** Time-dependent changing polarization in CIPS, where intralayer and interlayer switching associated double-peak function is responsible for the distribution of switching time.

https://doi.org/10.1038/s41467-025-59697-z

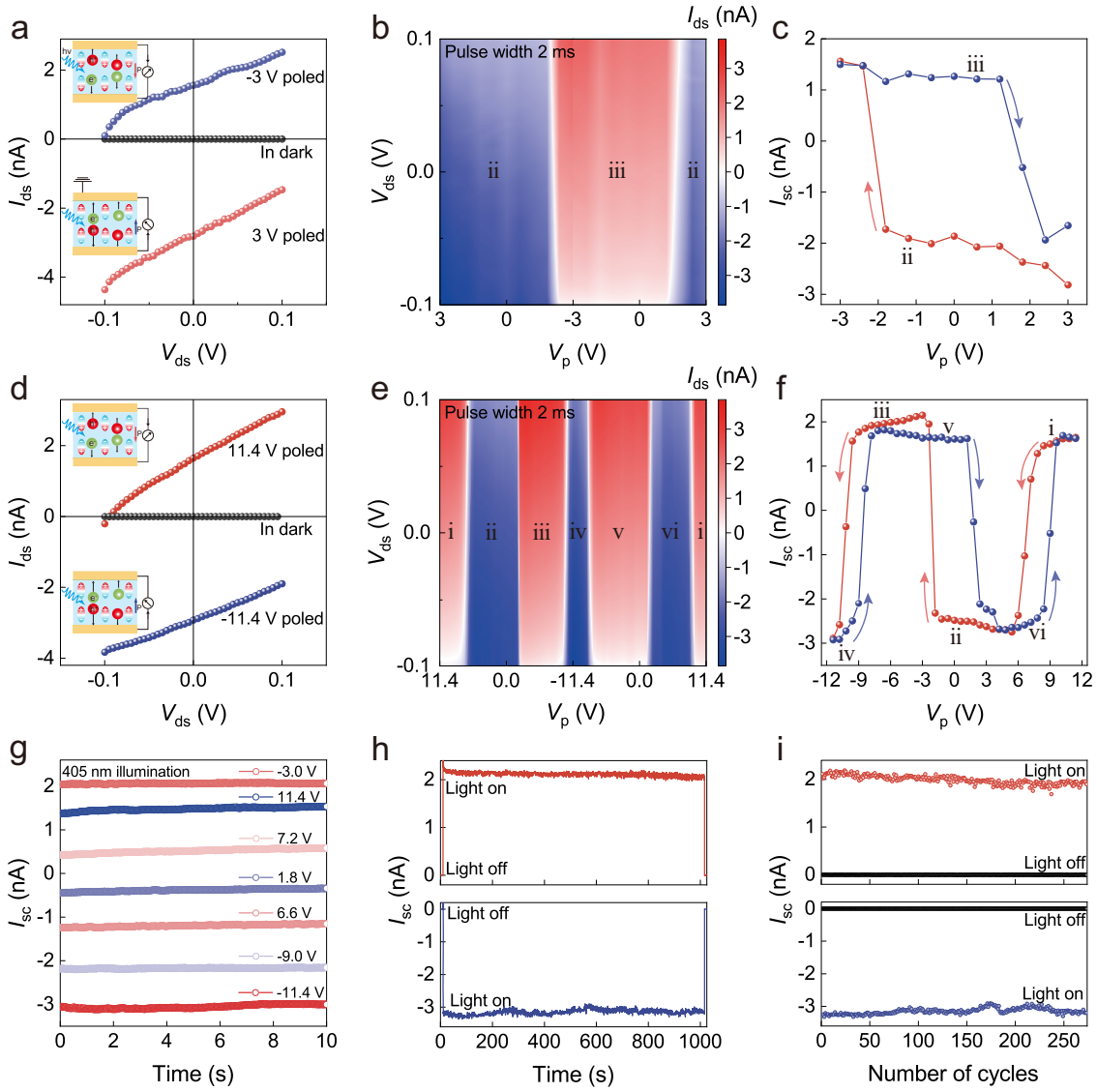

Fig. 2 | Anomalous FePV switching behavior in CIPS. a *I-V* characteristic of device under illumination after applying 3 V (−3 V) V_p, plotted by the red dots (blue dots). The black dots of *I-V* are measured in the dark condition. **b** Changing behaviors of photovoltaic current as V_p scans from 3 to −3 V and back to 3 V, with magnitude illustrated by a color map. **c** Extracted I_{sc} as a function of V_p from (**b**). **d** *I-V* characteristic of device under illumination after applying 11.4 V (−11.4 V) V_p, plotted by the red dots (blue dots). **e** Changing behaviors of photovoltaic current as V_p scans from 11.4 to −11.4 V and back to 11.4 V with a step of 0.6 V. **f** Extracted I_{sc} as a function of V_p from (**e**). **g** I_{sc} versus time of several typical polarization states in (**f**). **h** Retention characteristics of P_{down} (set by 11.4 V V_p, red line) and P_{up} (set by −11.4 V V_p, blue line) states. **i** Cycle-to-cycle measurement of I_{sc} at P_{down} and P_{up} states in (**h**).

kinetics of CIPS, we discovered three distinct switching modes depending on the Cu ions migration dynamics in ferroionic CIPS. Through precisely tuning the ion dynamics via the amplitude and width of poling voltage (V_p), we achieved configurable polarization switching, including digital switching, gradual switching, and accumulative switching in a single device. This work unlocks new possibilities for innovative ferroelectric device types based on the ferroionic material system.

Results

Anomalous ferroelectric photovoltaic switching in CIPS

For characterizing the polarization switching kinetics in CIPS thin films, the conventional positive-up-negative-down (PUND) method is invalid[40], as the polarization-switching current is obscured by leakage current[2,36–39]. To avoid the effect of ion migration and electron tunneling, FePV measurement is adopted to characterize the polarization states (see Methods for details). When polarized CIPS is upon the laser illumination, a polarization state determined short current (I_{sc}) is generated[16,41]. FePV I_{sc} actually provides an effective way to quantify the remanent polarization[16] (discussed in Supplementary Notes 2 and 3). For this reason, few-layered graphene is utilized as the transparent electrodes, and FePV measurement of a sandwiched graphene/CIPS/graphene device is performed. The device fabrication is described in the methods, and CIPS crystal-growth and the materials characterizations are shown in Supplementary Fig. 1 and Supplementary Fig. 2. During the measurement, both poling and reading voltage are applied to the bottom graphene electrode (Supplementary Fig. 3), and the sweeping range of read voltage is limited to 0.1 V to avoid disturbing the polarization. A positive pulse of 3 V (V_p = 3 V) or a negative pulse of −3 V (V_p = −3 V) is carried out to poling the device. The pulse width is 2 ms, a typical duration required for polarization switching in CIPS[30,42]. After that, the current-voltage (*I-V*) curves of the device under illumination are measured. We can see from the results in Fig. 2a that I_{sc} is negative at 3 V V_p but positive at −3 V V_p. Moreover, as V_p decreases from 3 to −3 V and then increases back to 3 V with step of

0.6 V, the monitored photovoltaic current changes from negative to positive one at about −2 V V_p and then changes back to negative one at about 2 V V_p (Fig. 2b). The extracted I_{sc} as function of V_p (I_{sc}-V_p) is depicted in Fig. 2c, showing a typical ferroelectric switching associated clockwise hysteresis behavior. The amplitude of coercive voltages (V_c), related to switching from upward polarization (P_{up}) to downward polarization (P_{down}) or switching from P_{down} to P_{up}, are both about 2 V.

Surprisingly, while V_p increases from 3 to 11.4 V, in contrast to the result in Fig. 2a, a completely reversed *I-V* characteristic is observed. I_{sc} is positive at 11.4 V V_p but becomes negative at −11.4 V V_p (Fig. 2d). Given that I_{sc} is opposite to the direction of polarization dipoles, the results in Fig. 2d indicate P_{down} and P_{up} are even achieved through applying a positive and a negative V_p, respectively. To further characterize such anomalous FePV behavior, a cycling scanning V_p ranged from 11.4 to -11.4 V with a step of 0.6 V is performed. It is found that the phase of I_{sc} even switches six times during V_p cycling scanning, as shown in Fig. 2e. The corresponding open-circuit voltage (V_{oc}) as a function of V_p also shows a 6-times switching behavior (Supplementary Fig. 4). The extracted I_{sc}-V_p in Fig. 2f shows an interesting feature of three clear hysteresis windows. As V_p backward decreases from 11.4 to −11.4 V and then forward increases from −11.4 to 11.4 V, I_{sc} sequentially changes from state i to state iv (i→ii→iii→iv) first, and following changes from iv back to i (iv→v→vi→i). Here, featuring I_{sc} from state ii to state iii with V_p backward scanning and I_{sc} from state v to state vi with V_p forward scanning, forms a hysteresis window. Such hysteresis window can be well tuned by changing the pulse width of V_p (Supplementary Fig. 5). It is found that the difference of I_{sc} between state v and state ii decreases and even near disappears as pulse width increases to 40 ms, but the critical voltage at which I_{sc} sharp changes almost keep unchanged, with amplitude of ~2 V. The value is similar with the V_c in Fig. 2c, indicating the intrinsic ferroelectric switching should be responsible for the hysteresis window near 0 V V_p.

To further confirm the photoelectric response of the device, the time-dependent I_{sc} was also monitored, providing an effective method to demonstrate the retention and stability of polarization. I_{sc} versus time of several typical states in Fig. 2f are illustrated in Fig. 2g. The results indicate that the polarization remains almost unchanged while applying laser illumination. Furthermore, Fig. 2h characterizes the retention of CIPS FePV, where the polarization was set as P_{down} and P_{up} by 11.4 and −11.4 V V_p, respectively. I_{sc} remains well more than 1000 s, indicating a great potential for achieving long optoelectronic storage. Through turning on and off the laser repeatedly, the cycle-to-cycle measurement of I_{sc} was performed. The result in Fig. 2i demonstrates that such anomalous I_{sc} is fairly robust, with a negligible change over 250 cycles. The detailed mechanism will be discussed in the following section.

Mechanism of anomalous FePV behavior

To further confirm the FePV characteristics of CIPS, ten-times repetitive V_p with various amplitudes have been employed to poling the device. As shown in Fig. 3a, the device was first reset by 11.4 V V_p with a width of 2 ms (11.4 V, 2 ms) to obtain P_{down} state. It is found that for 3 and −11.4 V V_p, once the first voltage pulse is applied, I_{sc} sharply decreases from 2 nA to one less than −2 nA, indicating the polarization is being switched from P_{down} to P_{up}. Meanwhile, P_{down} keeps almost unchanged while -3 V V_p is applied repetitively. Thus, it demonstrates that two E_c with opposite polarity, including a polarization alignment parallel E_{c1} with small amplitude and a polarization alignment anti-parallel E_{c2} with large amplitude, are responsible for the switching from P_{down} to P_{up}. Similarly, two E_c are also observed as polarization is switched from P_{up} to P_{down} (Fig. 3b). These two coercive fields associated polarization switching, are also identified by the switching spectroscopy piezoresponse forece microscopy (SS-PFM) and PFM mapping measurement (Supplementary Fig. 6).

Theoretical and experimental studies demonstrate that due to the Cu ions migration, Cu ions hopping in CIPS happens not only within the single layer but also across the vdW gaps, namely intralayer hopping and interlayer hopping, respectively. Combining with the two hopping progresses, Cu ions long migration happens. Such long migration and accumulation of Cu ions on one side of electrode, even induce a photovoltaic I_{sc} (Supplementary Fig. 7), but the polarity of I_{sc} is opposite to that of case at large V_p in Fig. 3a, b. By contrast, as Cu ions hop across the vdW gap merely, polarization aligns against the direction of the applied electric field[32], leading to a depolarization electric field whose direction is in agreement with the polarity of I_{sc} observed in Fig. 2d. Thus, the individual interlayer hopping rather than Cu ions long migration is more desirable for the anomalous FePV I_{sc} (Supplementary Fig. 8). Although the energy barrier for hopping across the vdW gap is much higher than hopping within the single layer, nearly half that could be reduced through sequential switching[35]. Indeed, the intermediate states beneficial to sequential switching are widely observed in our CIPS device (Supplementary Fig. 9). Besides, a plentiful supply of Cu vacancies and interstitials can also effectively facilitate such interlayer hopping[33,35]. Therefore, it is reasonable to infer that the two coercive fields, E_c involved switching characteristics origin from intralayer and interlayer switching progress, respectively. That is, the polarization alignment parallel to E_{c1} is responsible for intralayer switching and the polarization alignment anti-parallel to E_{c2} is responsible for interlayer switching, respectively.

Based on the above analysis, the physical scenario of anomalous FePV behaviors can be illustrated in Fig. 3c. In our device, the obtained P_{down} and P_{up} states actually contain low polarization (LP) and high polarization (HP)[28], as supported by PFM mapping measurement in Supplementary Fig. 9. Here, for simplicity, the downward polarization (−LP/−HP) and upward polarization (+LP/+HP) are uniformly named P_{down} and P_{up}, respectively. To conveniently display the Cu ions' intralayer and interlayer hopping progress, we focus on the initial Cu ions distribution in layer-1, denoted by the black dashed box, while applying cyclic scanning V_p. After applying a stimulus of 11.4 V V_p, the initial polarization state is set as P_{down}, with most of Cu ions accumulate at the bottom of layer-1. When a positive V_p with an electric field amplitude larger than E_{c1}, is applied subsequently, these Cu ions hop from the bottom to the top of layer-1. These Cu ions keep located at top sites until a negative V_p with electric filed amplitude larger than E_{c1} is applied, at which these Cu ions hop back to the bottom of layer-1 (Fig. 3c). The almost same I_{sc} at state (i) and state (iii) confirms that the corresponding polarization states of them are similar. Next, as a more negative V_p with electric field amplitude larger than E_{c2} is applied, these Cu ions at the bottom of layer-1 hop even across the vdW gap to the top of layer-2. At that time, polarization is unusually switched from P_{down} to P_{up}, against the applied electric field. After that, applying forward scanning V_p, similar with the progress from state (i) to state (iv), Cu ions sequentially undergoes hopping from the top to bottom of layer-2 (iv→v), hopping from the bottom to top of layer-2 (v→vi), and hopping from the top of layer-2 across to the bottom of layer-1 (vi→i). Thus, the hysteresis window near zero V_p in Fig. 2f attributes to the intralayer switching. Importantly, during the progress from state i to state ii (from state iv to state v), the intralayer switching dominates, in contrast to the progress from state vi to state i (from state iii to state iv), where interlayer switching dominates. As a result, a small V_p is required for the former while a large V_p is required for the latter, forming two hysteresis windows. Such a typical hysteresis loop with six-times switching behaviors, is also observed in the SS-PFM measurement (Supplementary Fig. 6), further providing cross validation that polarization switching between upward and downward directions alternatively occurs six times while applying cyclic scanning voltage. So far, the anomalous FePV behaviors root in distinguishable Cu ions intralayer and interlayer hopping progress, indicating it is possible for characterizing the intralayer and interlayer switching kinetics.

https://doi.org/10.1038/s41467-025-59697-z

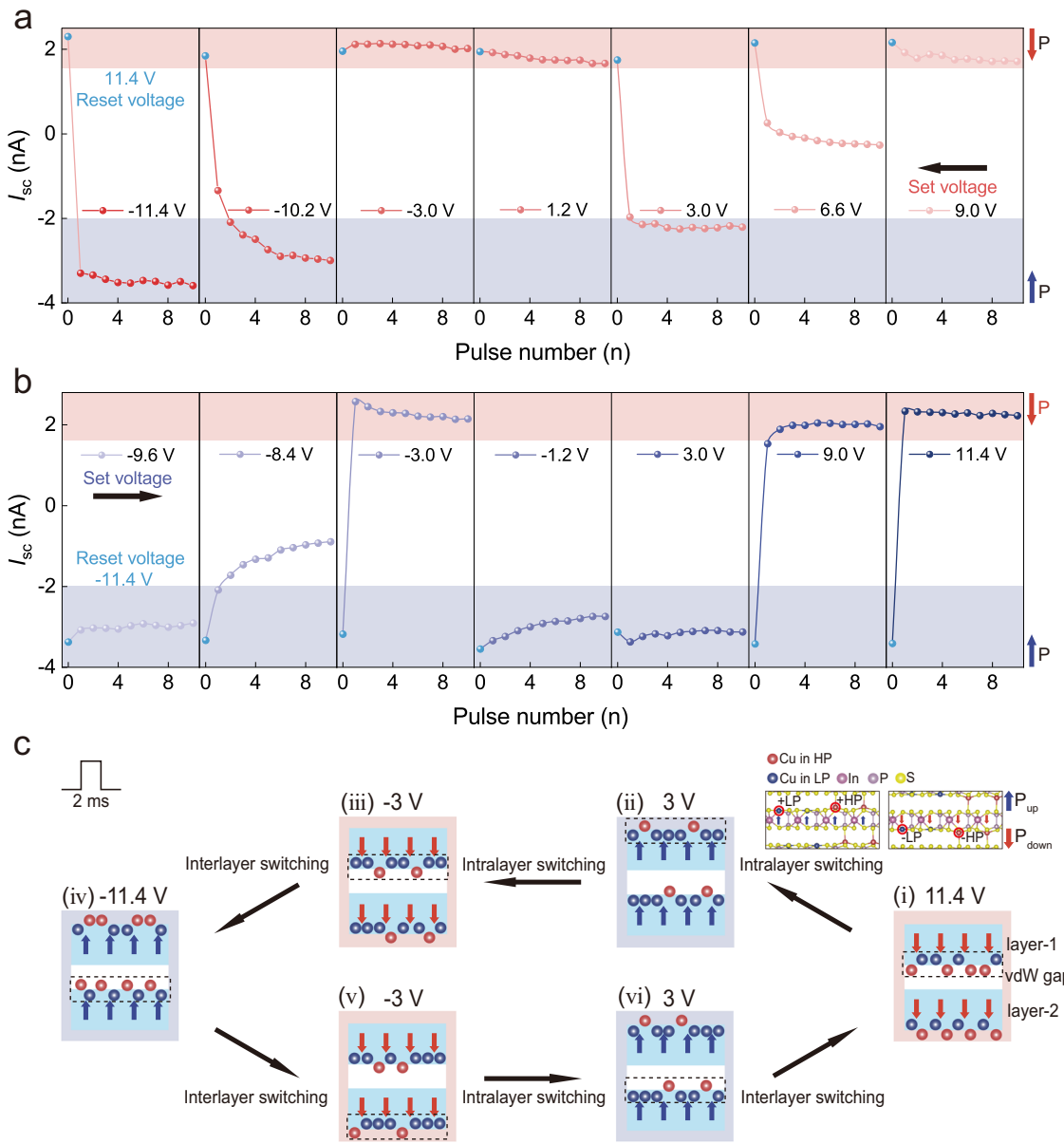

Fig. 3 | Switching mechanism of the anomalous FePV behavior in CIPS. **a** Response of I_{sc} while applying repetitive V_p with decreasing from 9 to −11.4 V. A V_p (11.4 V, 2 ms) is used as reset voltage to obtain an initial P_{down} state, denoted by red arrow. **b** Response of I_{sc} as the repetitive V_p increases from −9.6 to 11.4 V, where a V_p (−11.4 V, 2 ms) is adopted to reset the device, forming another initial P_{up} state, denoted by blue arrow. **c** Evolution of Cu ions distribution while applying cyclic scanning V_p, where the focused Cu ions are denoted by the black dashed box to present ion migration paths. Cu ions in LP and HP states are depicted by the blue and red spheres, respectively, and downward polarization (−LP/−HP) and upward polarization (+LP/+HP) are uniformly named P_{down} and P_{up}, illustrated in the inset.

Configurable polarization switching in CIPS

To further shed light on the switching kinetics of Cu ions intralayer and interlayer hopping progress, time-dependent I_{sc} measurement under various V_p were performed (Fig. 4). The device is initially set by 11.4 V, time evolution of I_{sc} under different V_p presents a tendency that I_{sc} gradually changes from positive to negative and then changes back to positive value (Fig. 4a). As V_p increases, the changing process becomes faster. Such a time-dependent twice switching process is further depicted in Fig. 4b. It indicates the ferroelectric polarization is switched from initial P_{down} to P_{up} for a short time, and gradually changes back to P_{down} for a long time. In other words, for a short time, the intralayer switching that from initial P_{down} to P_{up} dominates, but for a long time, interlayer switching gradually emerges and induces polarization changing back to P_{down}. The corresponding modes of polarization switching are named as Type I and Type II, respectively. Given that the dipole in CIPS owns independent switching progress, the NLS model is more appropriate for polarization switching kinetics[23] (see Supplementary Notes 2, 3). The extracted Lorentzian distribution functions at 4 V V_p is displayed in Fig. 4c. It is founded that the distribution function presents unique double-peak features, and the extracted switching time t_1 is one eighth of t_2. The evolution of log t_1 and log t_2 as a function of the inverse electric field follows the characteristic Merz's law[20,43] (Supplementary Fig. 10). Actually, during Type II switching progress, intralayer and interlayer switching are both involved. To reveal the individual interlayer switching progress, a reset voltage of −11.4 V is adopted to obtain the initial P_{up}. One can see from Fig. 4d, e that I_{sc} under different V_p monotonically increase from negative to positive value, with ferroelectric polarization is being switched from the initial P_{up} to P_{down} (named Type III switching mode). At 4 V V_p, the extracted switching time t_3 is about three times larger

https://doi.org/10.1038/s41467-025-59697-z

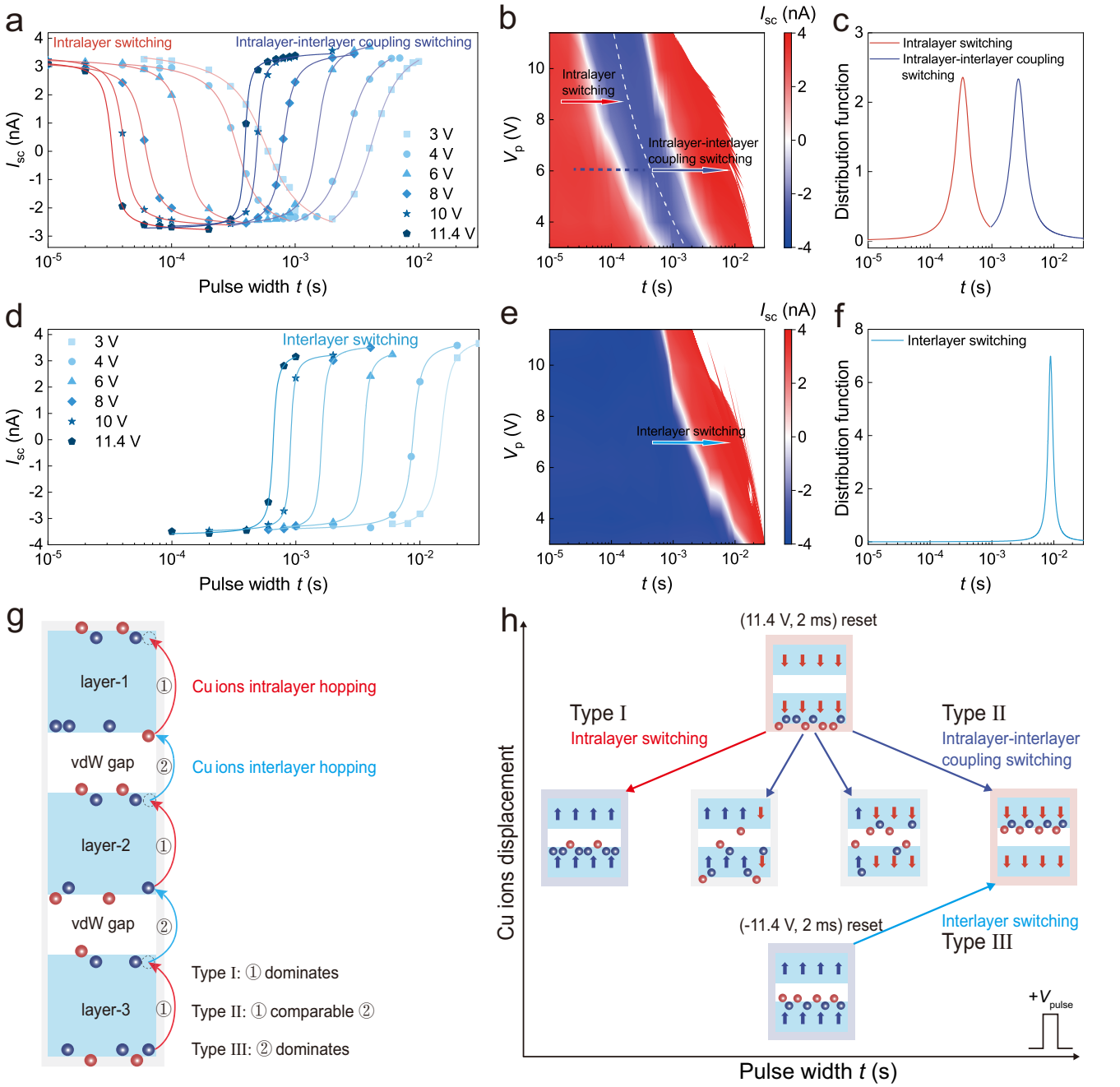

Fig. 4 | Polarization-switching kinetics in CIPS. a Measured I_{sc} as a function of pulse width at various V_p, where a V_p (11.4 V, 2 ms) is used as reset voltage to obtain an initial P_{down} state. The solid lines are the fitting curves. **b** Mapping plot of I_{sc} derived from (**a**), highlighting two distinct switching process that intralayer switching for a short time and intralayer-interlayer coupling switching for a long time. **c** Extracted Lorentzian distribution from (**a**) at 4 V V_p. **d** Measured I_{sc} versus pulse width at different V_p, with an initial P_{up} state through applying reset voltage V_p (−11.4 V, 2 ms). **e** Mapping plot of I_{sc} derived from (**d**). **f** Extracted Lorentzian distribution from (**d**) at 4 V V_p. **g** Diagram of Cu ions intralayer and interlayer hopping progress, of which dominates the switching process, resulting in the corresponding switching mode. **h** Time-dependent switching model of Type I, Type II, and Type III. The focused Cu ions on the bottom layer are used to describe their migration pathway in different switching modes.

than t_2, as plotted in Fig. 4f. The magnitudes of these extracted switching time value are consistent with the polarization switching in bulk CIPS[29] (Supplementary Figs. 10, 11). In addition, the extracted activation field and lower limit of switching time of these three switching modes, indicates interlayer switching should own the biggest energy barrier among them, which is further confirmed by the temperature-dependent FePV behaviors (Supplementary Fig. 12).

Due to the obtained polarization state is determined by the final static distribution of Cu ions, polarization reversal in CIPS should be determined by which of intralayer and interlayer hopping of Cu ions dominates, as depicted in Fig. 4g, h. That is to say, the switching kinetics of CIPS strongly depend on the distribution of Cu ions. For example, at an initial P_{up} condition, most of the Cu ions are located at the top of a single layer, and thus, the intralayer hopping does not occur due to the absence of bottom Cu ions. As pulse width increases, the interlayer hopping gradually emerges and dominates polarization reversal progress, forming Type III switching. By contrast, at an initial P_{down} condition, most of the Cu ions are located near the bottom of a

https://doi.org/10.1038/s41467-025-59697-z

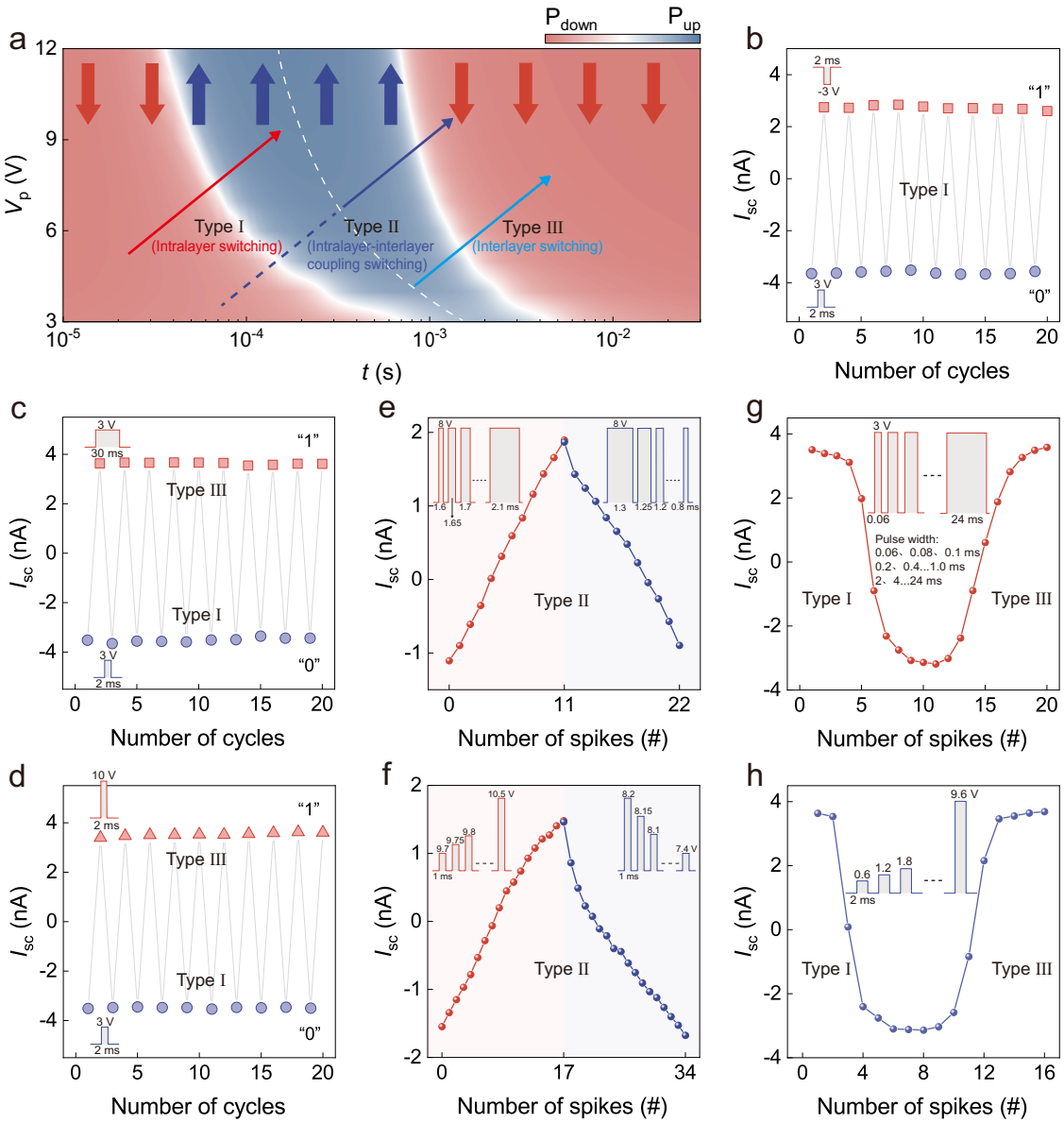

Fig. 5 | Device operation under configurable kinetics of polarization switching. **a** Simulated phase diagram of time and field-dependent polarization switching, where intralayer switching (Type I), intralayer-interlayer coupling switching (Type II), and interlayer switching (Type III) can be achieved by configuring V_p amplitude and width. **b** Typical digital memory of two distinct polarization states based on Type I switching model. **c** Digital memory behavior achieved by applying 3 V V_p with different durations. **d** Digital memory behavior achieved by unidirectional V_p with different amplitudes. **e**, **f** Gradual switching based on Type II switching mode through tuning the pulse width (**e**) and amplitude (**f**), respectively. **g**, **h** Accumulative switching achieved by designing pulse width (**g**) and amplitude (**h**), where Cu ions are gradually accumulated, driven by Type I switching, and subsequently released, driven by Type III switching.

single layer. For a V_p with short width, the intralayer hopping happens first and dominates the polarization reversal progress, resulting in Type I switching. While extending the duration of V_p, Cu ions hop from the bottom to top of this single layer and a part of these top Cu ions further hop across the vdW gap towards upper layer simultaneously, resulting in the intralayer and interlayer coupled Type II switching. Under this switching mode, the coupling between the intralayer and interlayer, depending on the Cu ions occupation distribution, can be feasibly tuned by the V_p amplitude and width, resulting in various polarization states (Fig. 4h), beneficial for ferroelectric multifunctional design.

Based on the understanding of configurable ferroelectric switching kinetics of CIPS, the polarization switching phase diagram depending on the V_p amplitude and width is theoretically simulated as shown in Fig. 5a (see Supplementary Note 2). Through configuring the V_p pulse amplitude and width, three modes of intralayer switching (Type I), intralayer-interlayer coupling switching (Type II), and interlayer switching (Type III) are available for designing ferroelectric devices. Utilizing Type I switching mode by applying 3 and −3 V V_p with a width of 2 ms, a typical digital memory with sharp switching between two distinct polarization states of P_{up} and P_{down} is achieved (Fig. 5b). Here, the negative I_{sc} and positive I_{sc} are used as the logic state "0" and logic state "1", respectively. Importantly, departs from conventional ferroelectric digital memory, such P_{up} and P_{down} involved binary digital memory even can be tuned through applying unidirectional V_p as depicted in Fig. 5c, d. As the polarization is switched to P_{up} states by a setting voltage V_p (3 V, 2 ms), a V_p with a longer width (3 V, 30 ms) or a V_p with a larger amplitude (10 V, 2 ms) is adopted as reset voltage to force P_{up} to switch back to P_{down} states. In this way, the switching behaviors that from P_{up} to P_{down} driven by Type III switching or from

P_{down} to P_{up} driven by Type I switching alternately happens. Notably, the endurance of the anomalous interlayer switching in Type III is over 10^4 cycles (Supplementary Fig. 13), facilitating the logical application.

The unique intralayer-interlayer coupling switching mechanism provides an effective way to precisely tune the distribution of Cu ions at the top and bottom layers, facilitating the achievement of multiple intermediate polarization states. As a series of V_p with increasing width from 1.6 to 2.1 ms is applied to the device, interlayer hopping progress is continuously enhanced while intralayer hopping progress is continuously reduced, making the total polarization states downward gradually. By contrast, through applying a series of V_p with decreasing width from 1.3 ms to 0.8 ms, interlayer hopping progress is gradually suppressed while intralayer hopping progress is increasingly enhanced, forming an upward polarization state (Fig. 5e). Similar behaviors are also achieved by applying a series of V_p with changing amplitude (Fig. 5f). Such gradually switching behavior is promising for implementing long-term potentiation (LTP) and long-term depression (LTD) of synaptic device.

In addition, configuring V_p with a larger range of increasing width (or a larger range of increasing amplitude), Cu ions could be tuned to continuously accumulate to top of layers through Type I switching and then release to upper layer through Type III switching, achieving an accumulative switching behavior (Fig. 5g, h). One can see that when the width of V_p increases progressively from 0.06 to 24 ms, I_{sc} gradually decreases from 3.5 to −3 nA within ten pulses, then increases back to 3.5 nA. This accumulation and releasing progress involved switching behaviors paved the way for mimicking biological neurons[44–46]. These cyclic intralayer and interlayer switching behaviors cause Cu ions to gradually accumulate or be released. The three modes of ferroelectric switching provide a platform for achieving binary switching, gradual switching, and accumulative switching in a single device.

Discussion

In summary, taking advantage of FePV behaviors, polarization switching kinetics of CIPS have been systematically investigated. It is found that FePV in CIPS presents an anomalous switching behavior, in which the phase of I_{sc} switches six times for cyclic scanning V_p. Such anomalous FePV behavior origins from the ion hopping with the intralayer process at a small V_p and the interlayer process at a large V_p. Polarization-switching kinetics in CIPS presents three switching modes, including intralayer switching, intralayer-interlayer coupling switching, and interlayer switching. Configuring the V_p amplitude and width provides a way to tune the switching kinetics in ferroionic CIPS, achieving multiple polarization switching modes in a single device. The ion migration modulated polarization switching kinetics paves the way for the development of advanced multifunctional ferroelectric devices, highlighting the potential of combining the ferroelectric and ion transport characteristics.

Methods

Characterization of CIPS single-crystal

The as-grown crystals were characterized by X-ray diffraction (XRD) patterns. Energy dispersive X-ray spectroscopy was adopted to characterize the homogeneity and composition of the CIPS films obtained by mechanical exfoliation. The ferroelectric phase of as-grown CIPS crystals is further confirmed by the Raman spectroscopy (HORIBA LabRAM Odyssey Raman spectrometer).

Fabrication of the device

The $CuInP_2S_6$ crystals were synthesized via chemical vapor transport method (Supplementary Fig. 1). Mechanical exfoliation was employed to prepare hexagonal boron nitride (h-BN), few layer graphene and CIPS flakes, and a vertical structure of graphene/CIPS/graphene/h-BN was fabricated by stacking these flakes on 285 nm SiO_2 substrate. After that, metal electrodes (Cr 8 nm/Au 50 nm) were introduced on graphene by lithography and electron beam evaporation.

Electrical measurement

The electrical measurement was performed by using an FS-Pro 380 semiconductor parameter analyzer, with the device placed in a high vacuum probe station (less than 1×10^{-3} Pa). The specific measurement steps of ferroelectric photovoltaic (FePV) are as follows: A poling voltage (V_p) was applied at the bottom graphene electrode to set the polarization state in the dark firstly, while the top graphene electrode was grounded. Subsequently, with laser illumination, *I-V* sweeping with a limited range of 0.1 V was adopted to obtain the FePV characteristic curves. In addition, the time-dependent short-current (I_{sc}) at zero bias voltage was also monitored. Upon the 405 nm laser illumination, numerous carriers were generated, and I_{sc} sharply increases from the noise level (1×10^{-13} A) to the magnitude of nA level. Given the CIPS bandgap of ~2.8 eV (Supplementary Fig. 2b), a 405 nm laser diode with a fixed light intensity of about 1.2 mW was used as the excitation source.

Atomic force microscope (AFM) measurement

AFM was performed on the Asylum Research Cypher S system using the PPP-EFM probe from NANOSENSORS™, with a spring constant of 2.8 N/m and a free resonance frequency of 75 kHz.

Piezoelectric force microscopy (PFM) measurement

PFM was performed on the Asylum Research Vero ES system using the PPP-EFM conductive probe, with a spring constant of 2.8 N/m and a free resonance frequency of 75 kHz. The Vero ES PFM is equipped with a quadrature phase differential interferometry (QPDI) detector, and makes measuring the accurate displacement of the probe tip available. Notably, the data presented in Supplementary Fig. 6f were acquired using the Asylum Research Cypher S system, employing the same type of PPP-EFM conductive probe with identical specifications. In this work, datasets obtained from the Cypher S system are explicitly indicated in the figure captions. Unless otherwise specified, all other PFM measurements were performed using the Asylum Research Vero ES system.

Data availability

All data supporting the findings of this study are available within the article and its Supplementary Information files.

References

1. Si, M. et al. A ferroelectric semiconductor field-effect transistor. *Nat. Electron.* **2**, 580–586 (2019).
2. Wu, J. et al. High tunnelling electroresistance in a ferroelectric van der Waals heterojunction via giant barrier height modulation. *Nat. Electron.* **3**, 466–472 (2020).
3. Wang, X. et al. Van der Waals engineering of ferroelectric heterostructures for long-retention memory. *Nat. Commun.* **12**, 1109 (2021).
4. Kim, W. Y. et al. Graphene-ferroelectric metadevices for nonvolatile memory and reconfigurable logic-gate operations. *Nat. Commun.* **7**, 10429 (2016).
5. Yin, X., Chen, X., Niemier, M. & Hu, X. S. Ferroelectric FETs-based nonvolatile logic-in-memory circuits. *IEEE T. VLSI Syst.* **27**, 159–172 (2018).
6. Khan, A. I., Keshavarzi, A. & Datta, S. The future of ferroelectric field-effect transistor technology. *Nat. Electron.* **3**, 588–597 (2020).
7. Wang, J. et al. Ferroelectric domain-wall logic units. *Nat. Commun.* **13**, 3255 (2022).
8. Park, S. E. et al. Relaxor based ferroelectric single crystals for electro-mechanical actuators. *Mater. Res. Innov.* **1**, 20–25 (1997).

9. Zhou, X. F. et al. Lead-free ferroelectrics with giant unipolar strain for high-precision actuators. *Nat. Commun.* **15**, 6625 (2024).
10. Muralt, P. Ferroelectric thin films for micro-sensors and actuators: a review. *J. Micromech. Microeng.* **10**, 136 (2000).
11. Choi, T., Lee, S., Choi, Y. J., Kiryukhin, V. & Cheong, S. W. Switchable ferroelectric diode and photovoltaic effect in $BiFeO_3$. *Science* **324**, 63–66 (2009).
12. Yang, S. et al. Above-bandgap voltages from ferroelectric photovoltaic devices. *Nat. Nanotechnol.* **5**, 143–147 (2010).
13. Guo, R. et al. Non-volatile memory based on the ferroelectric photovoltaic effect. *Nat. Commun.* **4**, 1990 (2013).
14. Butler, K. T., Frost, J. M. & Walsh, A. Ferroelectric materials for solar energy conversion: photoferroics revisited. *Energ. Environ. Sci.* **8**, 838–848 (2015).
15. Spanier, J. E. et al. Power conversion efficiency exceeding the Shockley-Queisser limit in a ferroelectric insulator. *Nat. Photonics* **10**, 611–616 (2016).
16. Li, Y. et al. Enhanced bulk photovoltaic effect in two-dimensional ferroelectric $CuInP_2S_6$. *Nat. Commun.* **12**, 1–7 (2021).
17. Scott, J. F. & Paz de Araujo, C. A. Ferroelectric memories. *Science* **246**, 1400–1405 (1989).
18. Vizdrik, G., Ducharme, S., Fridkin, V. M. & Yudin, S. G. Kinetics of ferroelectric switching in ultrathin films. *Phys. Rev. B* **68**, 094113 (2003).
19. Jerry, M. et al. Ferroelectric FET analog synapse for acceleration of deep neural network training. In *2017 IEEE International Electron Devices Meeting* (*IEDM*) 6.2. 1–6.2. 4 (IEEE, 2017).
20. Boyn, S. et al. Learning through ferroelectric domain dynamics in solid-state synapses. *Nat. Commun.* **8**, 14736 (2017).
21. Oh, S., Hwang, H., & Yoo, I. K. Ferroelectric materials for neuromorphic computing. *APL Mater.* **7**, 091109 (2019).
22. Tagantsev, A. K., Stolichnov, I., Setter, N., Cross, J. S. & Tsukada, M. Non-Kolmogorov-Avrami switching kinetics in ferroelectric thin films. *Phys. Rev. B* **66**, 214109 (2002).
23. Jo, J. et al. Domain switching kinetics in disordered ferroelectric thin films. *Phys. Rev. Lett.* **99**, 267602 (2007).
24. Ni, K. et al. A novel ferroelectric superlattice based multi-level cell non-volatile memory. In *2019 IEEE International Electron Devices Meeting* (*IEDM*) 28.28. 21–28.28. 24 (IEEE, 2019).
25. Maisonneuve, V., Cajipe, V. B., Simon, A., Von Der Muhll, R. & Ravez, J. J. P. R. B. Ferrielectric ordering in lamellar $CuInP_2S_6$. *Phys. Rev. B* **56**, 10860 (1997).
26. Liu, F. et al. Room-temperature ferroelectricity in $CuInP_2S_6$ ultrathin flakes. *Nat. Commun.* **7**, 1–6 (2016).
27. You, L. et al. Origin of giant negative piezoelectricity in a layered van der Waals ferroelectric. *Sci. Adv.* **5**, eaav3780 (2019).
28. Brehm, J. A. et al. Tunable quadruple-well ferroelectric van der Waals crystals. *Nat. Mater.* **19**, 43–48 (2020).
29. Zhou, S. et al. Anomalous polarization switching and permanent retention in a ferroelectric ionic conductor. *Mater. Horiz.* **7**, 263–274 (2020).
30. Neumayer, S. M. et al. Ionic control over ferroelectricity in 2D layered van der Waals capacitors. *ACS Appl. Mater. Interfaces* **14**, 3018–3026 (2022).
31. O'Hara, A., Balke, N. & Pantelides, S. T. Unique features of polarization in ferroelectric ionic conductors. *Adv. Electron. Mater.* **8**, 2100810 (2022).
32. He, R. et al. Unconventional ferroelectric domain switching dynamics in $CuInP_2S_6$ from first principles. *Phys. Rev. B* **108**, 024305 (2023).
33. Neumayer, S. M. et al. Alignment of polarization against an electric field in van der Waals ferroelectrics. *Phys. Rev. Appl.* **13**, 064063 (2020).
34. Neumayer, S. M. et al. The concept of negative capacitance in ionically conductive van der Waals ferroelectrics. *Adv. Energy Mater.* **10**, 2001726 (2020).
35. Seleznev, D., Singh, S., Bonini, J., Rabe, K. M. & Vanderbilt, D. Cyclic ferroelectric switching and quantized charge transport in $CuInP_2S_6$. *Phys. Rev. B* **108**, L180101 (2023).
36. Li, B. et al. An electronic synapse based on 2D ferroelectric $CuInP_2S_6$. *Adv. Electron. Mater.* **6**, 2000760 (2020).
37. Zhang, D. et al. Anisotropic ion migration and electronic conduction in van der Waals ferroelectric $CuInP_2S_6$. *Nano Lett.* **21**, 995–1002 (2021).
38. Chen, J. et al. Mimicking neuroplasticity via ion migration in van der Waals layered copper indium thiophosphate. *Adv. Mater.* **34**, 2104676 (2022).
39. Jiang, X. et al. Manipulation of current rectification in van der Waals ferroionic $CuInP_2S_6$. *Nat. Commun.* **13**, 574 (2022).
40. Kim, Y. et al. Non-Kolmogorov– Avrami– Ishibashi switching dynamics in nanoscale ferroelectric capacitors. *Nano Lett.* **10**, 1266–1270 (2010).
41. Bai, Y. et al. Anomalous photocurrent reversal for the same polarization direction in van der Waals ferroelectric $CuInP_2S_6$. *PRX Energy* **3**, 023004 (2024).
42. Zhang, Y. et al. Switchable out-of-plane shift current in ferroelectric two-dimensional material $CuInP_2S_6$. *Appl. Phys. Lett.* **120**, 013103 (2022).
43. Li, J. et al. Reproducible ultrathin ferroelectric domain switching for high-performance neuromorphic computing. *Adv. Mater.* **32**, 1905764 (2020).
44. Mulaosmanovic, H., Chicca, E., Bertele, M., Mikolajick, T. & Slesazeck, S. Mimicking biological neurons with a nanoscale ferroelectric transistor. *Nanoscale* **10**, 21755–21763 (2018).
45. Mulaosmanovic, H. et al. Investigation of accumulative switching in ferroelectric FETs: enabling universal modeling of the switching behavior. *IEEE T. Electron Dev.* **67**, 5804–5809 (2020).
46. Mikolajick, T., Park, M. H., Begon-Lours, L. & Slesazeck, S. From ferroelectric material optimization to neuromorphic devices. *Adv. Mater.* **35**, 2206042 (2023).

Acknowledgements

The authors appreciate Weijia Ren and Aijun Zhou from the Analysis and Testing Center, University of Electronic Science and Technology of China, for technical support. This work was supported by the National Key Research & Development Program: 2020YFA0309200 (F.L.), 2023YFA1607102 (G.C.); the National Natural Science Foundation of China: 92477115 (F.L.), 12161141015 (F.L.), 62074025 (F.L.), 62304183 (G.C.), 62374043 (W.L.); Sichuan Science and Technology Program: 2024YFHZ0264 (F.L.), 2024NSFSC1002 (Q.L.); Sichuan Province Key Laboratory of Display Science and Technology (F.L.); and Shanghai Oriental Talent Program-Youth Project: 2022 (W.L.).

Author contributions

F.L., W.L., and Y.K. supervised the project. F.L., W.L., G.C., and L.L. conceived the idea and designed the experiments. L.L. fabricated the device, performed the optoelectronic measurements, and, assisted by E.P., conducted the PFM characterization. G.C. and X.C. conducted the simulation. Q.L. prepared the single crystal. J.C., R.W., and B.D. assisted with the device fabrication. F.L., G.C., W.L., Y.K., and X.L. analyzed the data. G.C., L.L., and F.L. wrote the manuscript with input from all authors. All authors discussed the results.

Competing interests

The authors declare no competing interests.

Additional information

Supplementary information The online version contains supplementary material available at https://doi.org/10.1038/s41467-025-59697-z.

Correspondence and requests for materials should be addressed to Guiming Cao, Wenwu Li or Fucai Liu.

Peer review information *Nature Communications* thanks Suraj Cheema who co-reviewed with Piush BeheraChing-Hwa Ho and Yi-Chun Chen for their contribution to the peer review of this work. A peer review file is available.